Current Biology 19, 1833–1838, November 17, 2009 ©2009 Elsevier Ltd All rights reserved DOI 10.1016/j.cub.2009.09.025

Report

Dynein Antagonizes Eg5 by Crosslinking and Sliding Antiparallel Microtubules

Nick P. Ferenz,[1,2] Raja Paul,[3] Carey Fagerstrom,[1] Alex Mogilner,[3] and Patricia Wadsworth[1,2,*]
[1]Department of Biology
[2]Program in Molecular and Cellular Biology
University of Massachusetts Amherst, Amherst, MA 01003, USA
[3]Department of Neurobiology, Physiology, and Behavior and Department of Mathematics, University of California, Davis, Davis, CA 95616, USA

Summary

Mitotic spindle assembly requires the combined activity of various molecular motor proteins, including Eg5 [1] and dynein [2]. Together, these motors generate antagonistic forces during mammalian bipolar spindle assembly [3]; what remains unknown, however, is how these motors are functionally coordinated such that antagonism is possible. Given that Eg5 generates an outward force by crosslinking and sliding apart antiparallel microtubules (MTs) [4–6], we explored the possibility that dynein generates an inward force by likewise sliding antiparallel MTs. We reasoned that antiparallel overlap, and therefore the magnitude of a dynein-mediated force, would be inversely proportional to the initial distance between centrosomes. To capitalize on this relationship, we utilized a nocodazole washout assay to mimic spindle assembly. We found that Eg5 inhibition led to either monopolar or bipolar spindle formation, depending on whether centrosomes were initially separated by less than or greater than 5.5 μm, respectively. Mathematical modeling predicted this same spindle bistability in the absence of functional Eg5 and required dynein acting on antiparallel MTs to do so. Our results suggest that dynein functionally coordinates with Eg5 by crosslinking and sliding antiparallel MTs, a novel role for dynein within the framework of spindle assembly.

Results and Discussion

Eg5/Dynein Antagonism in LLC-Pk1 Cells

Before exploring the functional coordination of Eg5 and dynein, we first confirmed the antagonistic nature of these motors in LLC-Pk1 cells, as well as the relevance of this antagonism to spindle bipolarity [3]. To accomplish this, we treated metaphase cells expressing GFP-tubulin (LLC-Pk1α [7]) with monastrol to inhibit Eg5 [8] or injected them with p150-CC1 to inhibit dynein [9]. Immediately following monastrol treatment, bipolar spindles shortened by ~30% (see Figures S1A and S1C available online), but complete collapse into monopoles was not observed. Conversely, spindles lengthened by ~30% after dynein inhibition (Figures S1B and S1C). This spindle elongation was not a consequence of centrosome dissociation from spindle poles or mislocalization of Kif2a (unpublished data). Together, spindle shortening and lengthening following Eg5 and dynein inhibition, respectively, confirm the presence of an antagonistic relationship between these two motors in LLC-Pk1 cells.

We next monitored the response of Eg5-inhibited monopolar spindles to inhibition of dynein. LLC-Pk1α cells were treated with monastrol prior to nuclear envelope breakdown, and mitotic cells containing monopolar microtubule (MT) arrays were then injected with p150-CC1. In ~50% of such cells (13 of 30 cells), monopolar spindles reorganized into bipolar spindles (Figure S1D; Movie S1), defined here and subsequently as fusiform MT arrays, with the majority of chromosomes aligned between two distinct poles separated by a minimum of 5 μm. Bipolar spindles that formed following inhibition of Eg5 and dynein were morphologically and functionally equivalent to controls (Figure S2). Spontaneous bipolarization of monastrol-induced monopolar spindles was never observed, and injection of control antibodies left monopolar arrays unaltered (unpublished data), demonstrating the specificity of bipolarization to dynein inhibition.

The formation of bipolar spindles following inhibition of Eg5 and dynein demonstrates that an additional force drives pole separation. This force could be generated by MT polymerization [10] and/or additional plus-end-directed motors, such as Xklp2 [11]. Residual Eg5 activity, however, is unlikely to contribute to pole separation, given the efficacy of motor inhibition by monastrol [8]. In contrast, incomplete inhibition of dynein following injection of p150-CC1, which interferes with the dynein/dynactin interaction but not dynein's ATPase activity, could account for the observation that not all monopolar spindles were rescued. Finally, the geometry of MTs and chromosomes in coinhibited cells may influence the generation of pushing forces that restore spindle bipolarity.

In summary, the observation that dynein inhibition can rescue the monastrol-mediated monopolar phenotype demonstrates that an antagonistic balance between Eg5 and dynein contributes to the establishment of spindle bipolarity. Based on the evidence that Eg5 can slide apart overlapping MTs [4–6] and its antagonistic relationship with dynein [3], we hypothesize that dynein functions at regions of antiparallel overlap, where it crosslinks and slides antiparallel MTs in opposition to Eg5.

The Nocodazole Washout Assay as a Means to Study Eg5/Dynein Antagonism

If our hypothesis is valid, then dynein would likely be responsible for monopolar spindle formation in the presence of monastrol, because it would generate an inadequately opposed inward force. Because antiparallel overlap decreases as the distance between centrosomes increases (Figure S3A) and because the magnitude of our postulated dynein-mediated force would depend on the amount of antiparallel overlap, spindles that form in Eg5-inhibited cells should be resistant to collapse above a certain intercentrosomal threshold distance; in other words, spindles should exhibit an intercentrosomal-distance-dependent bistability. To examine this, we utilized a nocodazole washout assay [12], which generates mitotic cells containing centrosomes with widely variable positions (in a manner independent of the inhibitors present) (Figure S4).

*Correspondence: patw@bio.umass.edu

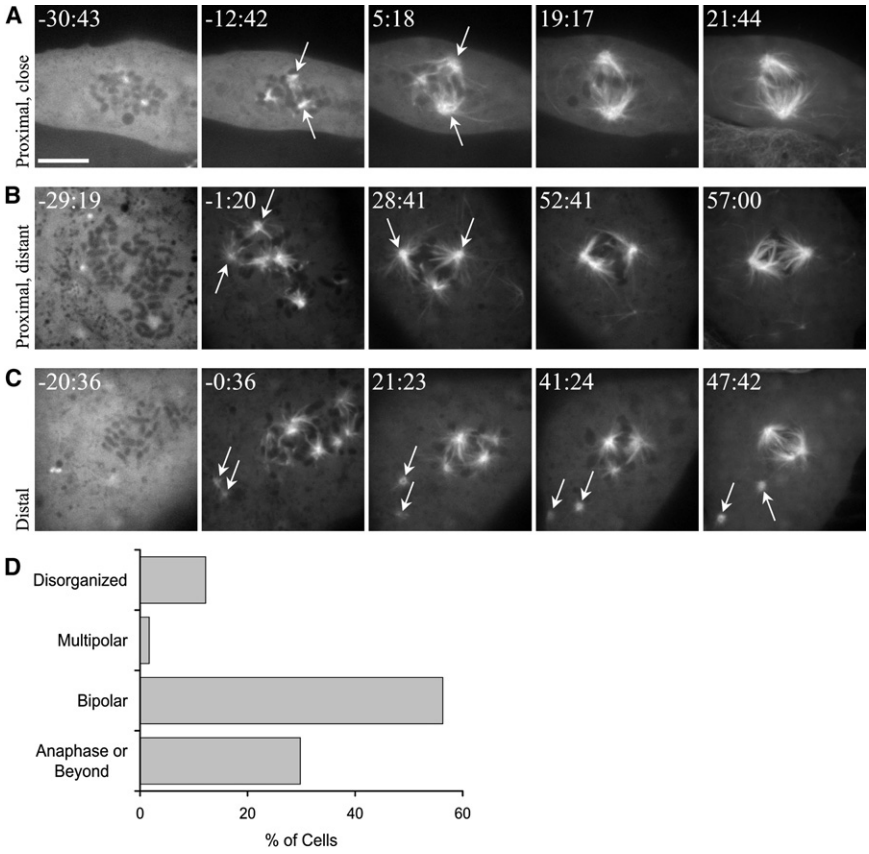

Figure 1. Spindle Assembly Following Nocodazole Washout

(A–C) Selected images from time-lapse sequences of cells treated with and released from nocodazole under the three centrosomal configurations. (A), (B), and (C) correspond to Movies S2, S3, and S4, respectively. In each case, a bipolar spindle assembles following nocodazole washout. In the first image of each sequence, centrosomes appear as white dots. Arrows subsequently mark the position of in-focus centrosomes when three or more foci are present. The last image of each sequence is a maximum-intensity projection. All times are relative to the final nocodazole washout (0:00) and are displayed as min:s.

(D) Percentage of fixed LLC-Pk1α cells at the indicated mitotic stages, present 60 min post-4× washout. Scale bar represents 10 μm.

In this assay, LLC-Pk1α cells were treated with nocodazole to completely disassemble MTs and were then washed four times with drug-free medium to initiate spindle assembly (see Experimental Procedures). Upon removal of drug, MTs assembled at centrosomes and chromosomes [12]. When centrosomal and chromosomal arrays were close enough to interact (proximal centrosomes), these MT populations quickly coalesced, ultimately resulting in bipolar spindles (9 of 13 cells; Figures 1A and 1B; Table S1; Movies S2 and S3); this occurred regardless of the initial spacing between proximal centrosomes. In cells with centrosomal arrays that failed to interact with the chromosomal array (distal centrosomes), acentrosomal bipolar spindles assembled around chromosomes (3 of 5 cells; Figure 1C; Table S1; Movie S4), confirming that mammalian chromosomes alone can organize MTs into bipolar structures [13, 14], even in the continued presence of centrosomes. Examination of cells fixed 60 min post-4×-washout revealed that ~30% had progressed into or beyond anaphase (Figure 1D), demonstrating that these bipolar spindles are functional and validating this assay as a tool for studying spindle assembly.

Monopolar Spindle Formation in Eg5-Inhibited Cells Requires Closely Associated Centrosomes

To test the potential bistability of forming spindles in Eg5-inhibited cells, we treated LLC-Pk1α cells first with nocodazole and subsequently with monastrol and then released them into monastrol-containing medium. As predicted, the initial spacing between proximal centrosomes had a profound effect on the resulting MT array. When proximal centrosomes were located close to one another (i.e., <5.5 μm apart), monopolar arrays of MTs formed following release from nocodazole (4 of 5 cells; Figure 2A; Movie S5). In striking contrast, however, when proximal centrosomes were located far from one another (i.e., >5.5 μm apart), bipolar arrays of MTs formed (6 of 7 cells; Figure 2B; Table S1; Movie S6). Furthermore, when centrosomes were distal, chromosomes organized short acentrosomal bipolar arrays in an Eg5-independent manner (3 of 4 cells; Figure 2C; Table S1); chromosomes also organized similar acentrosomal bipolar spindles in a dynein-independent manner (2 of 2 cells; Figure S5).

These data confirm the predicted intercentrosomal-distance-dependent bistability and suggest that the requirement for active Eg5 in establishing a bipolar spindle can be bypassed if spindle assembly initiates with well-separated centrosomes (i.e., >5.5 μm apart) or via an exclusively chromosomal pathway. In these cases, we expect the degree of antiparallel MT overlap to be insufficient to mediate dynein-dependent spindle collapse. Furthermore, our data show that Eg5 and dynein are each dispensable for acentrosomal bipolar spindle formation. Although chromosome-mediated spindle assembly following dynein inhibition has previously been noted [15], this is the first demonstration that Eg5 activity is likewise not required for this process.

Monopolar Spindle Formation in Eg5-Inhibited Cells with Closely Associated Centrosomes Requires Dynein Activity

Though intercentrosomal-distance-dependent spindle bistability supports our hypothesis, additional support can be obtained by confirming that dynein is responsible for spindle collapse in the presence of monastrol. To directly test this, we treated LLC-Pk1α cells first with nocodazole and monastrol and then injected them with p150-CC1 prior to release into monastrol-containing medium. Consistent with p150-CC1 injections into monastrol-treated monopoles, half of these cells (2 of 4 cells) bipolarized when proximal centrosomes were close to one another (Figure 3A; Table S1; Movie S7); the other half formed monopolar arrays. As expected, when proximal centrosomes were distant, 4 of 5 cells bipolarized (Figure 3B; Table S1). Acentrosomal bipolar arrays additionally formed in Eg5- and dynein-inhibited cells containing distal centrosomes (1 of 1 cell; Figure 3C; Table S1).

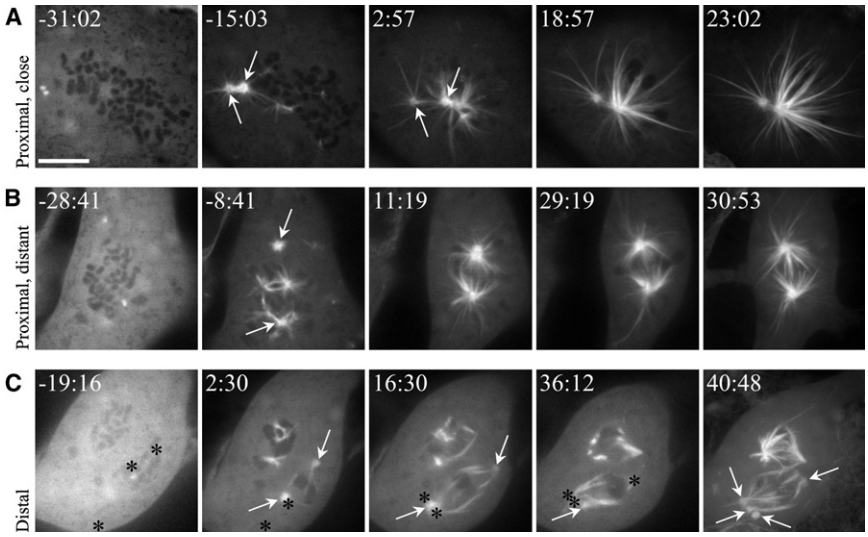

Figure 2. Spindle Bistability in the Absence of Eg5 Activity

Selected images from time-lapse sequences of cells treated with nocodazole and monastrol and then released into monastrol-containing medium. (A) and (B) correspond to Movies S5 and S6, respectively. Nocodazole washout leads to bipolar spindle formation, except when proximal centrosomes are close to one another. Setup is as defined in Figure 1. Additionally, asterisks mark the position of out-of-focus centrosomes. In (C), two mitotic cells have fused together; the top spindle is acentrosomal. Scale bar represents 10 μm.

These data reveal that monastrol-mediated spindle monopolarity is a dynein-dependent phenotype. Our results are therefore consistent with a model in which Eg5, located on antiparallel MTs, generates an outward sliding force that is resisted by a dynein-generated inward force also acting on antiparallel MTs. This is a novel role for dynein during spindle assembly, which has previously been suggested to exclusively crosslink parallel MTs [16], and is consistent with dynein's proposed role during *Xenopus* extract spindle fusion [17]. We predict specifically that dynein localizes and generates force at or near the plus ends of overlapping MTs, consistent with its plus-end localization in fungal systems [18, 19]. Here, dynein could crosslink MTs by binding to one MT via its stalk domain and to a second MT by a non-ATP-dependent interaction, mediated, for example, by proteins that bind both dynein and MTs. In strong support of this, recent work has shown that spindle assembly requires the MT-binding domain of the p150 subunit of dynactin [20] and that the MT plus-end-binding protein, CLIP-170, which binds to dynein, antagonizes Eg5 [3].

In Silico Modeling Confirms the Spindle Bistability of Eg5-Inhibited Cells

Although our in vivo data support our hypothesis that dynein localizes to and generates force at antiparallel MT overlap, confirmation of such necessarily involves visualizing both dynein and antiparallel MTs. In mammalian cells, however, the difficulties associated with genetically tagging and expressing dynein heavy chain preclude the former, whereas the density of spindle MTs obstructs the latter. We note, however, that dynein has been immunofluorescently localized to mammalian spindle MTs [21].

Despite these limitations, we can employ a mathematical model of spindle assembly to determine whether our in vivo results are consistent with dynein acting on antiparallel MTs. The following assumptions were made while constructing the model: (1) centrosomes nucleate asters consisting of tens to hundreds of MTs undergoing rapid dynamic instability, so that the MT length distribution is exponential [22]; (2) a few centrosomal MTs reach chromosome arms and generate a repulsive force (Figure 4A, force A), either by a polymerization ratchet or by interacting with chromokinesins; (3) a few centrosomal MTs reach the spindle equator, where Eg5 and dynein motors exert opposite sliding forces at the region of antiparallel overlap (Figure 4A, force B); and (4) tension generated at kinetochores pulls chromosomes toward centrosomes (Figure 4A, force C). Importantly, the precise location of dynein on antiparallel MTs (i.e., whether it is distributed along the whole overlap length or just at the plus ends) does not make a qualitative difference for the model's predictions.

These assumptions allow the effective outward force, *F*, applied to each centrosome to be computed as a function of

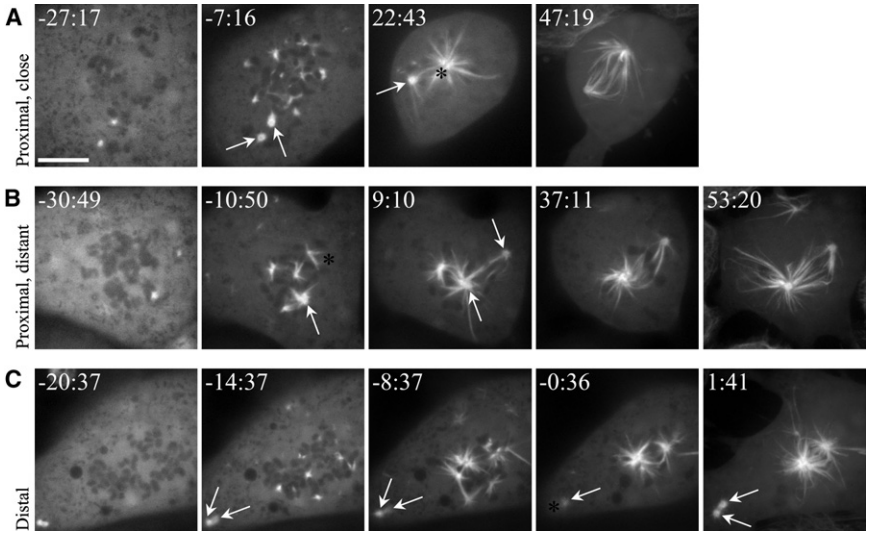

Figure 3. Dynein Is Required for Monopolar Spindle Formation

Selected images from time-lapse sequences of cells treated with nocodazole and monastrol, injected with p150-CC1, and then released into monastrol-containing medium. (A) corresponds to Movie S7. In each case, a bipolar spindle assembles after nocodazole washout. Setup is as defined in Figure 2. Scale bar represents 10 μm.

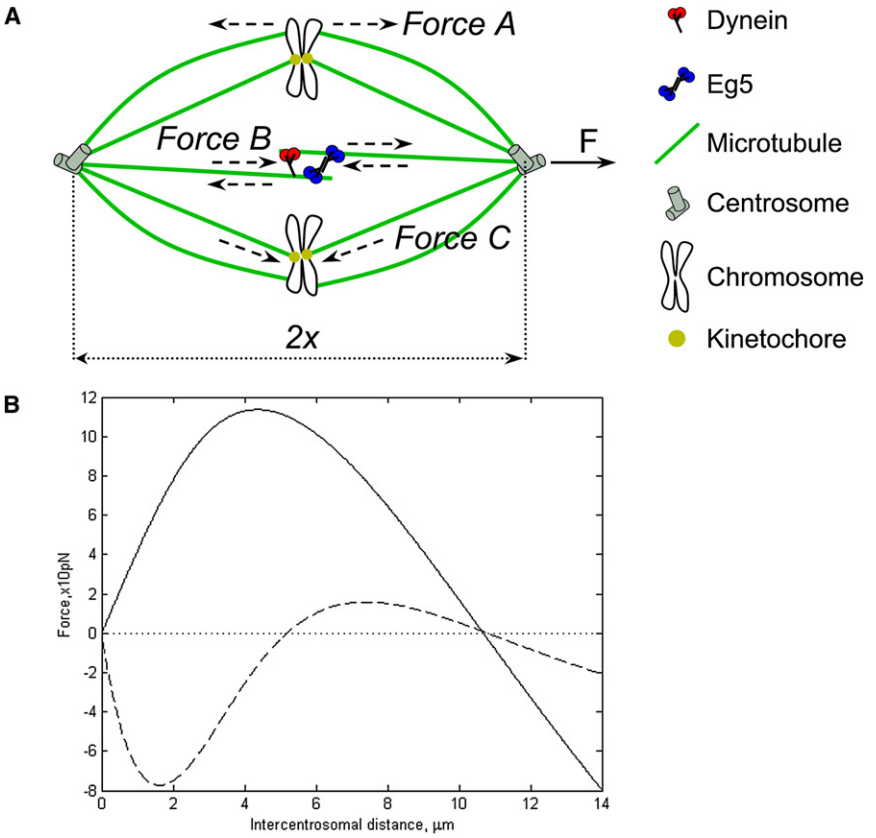

Figure 4. Mathematical Modeling

(A) Schematic of the mathematical model. The total force, *F*, acting on centrosomes is a function of forces A, B, and C (see text for description).

(B) Force versus intercentrosomal distance given by the model with a realistic chromosomal distribution at the spindle midplane (see Figure S6B) for $L = 2$, $A = 1$, and $C = 0.03$ for uninhibited, coinhibited (equation 4 in Supplemental Experimental Procedures, solid curve, $B = 0$), and Eg5-inhibited (equation 5 in Supplemental Experimental Procedures, dashed curve, $B = 2$) cells.

the half-spindle length, *x*, assuming that all chromosomes are crowded close together at the spindle equator (Figure 4A). This functional dependence has the form $F(x) = (Ae^{-x/L} - C) - 2Bxe^{-2x/L}$, where *L* is the average MT length, *A* is the maximal repulsive force on chromosome arms, *B* is the total motor force per unit length of antiparallel MT overlap, and *C* is the kinetochore tension force (see Supplemental Data). With this formula, we found that when parameter *B* was very small (i.e., when the outward sliding force by Eg5 and the inward pulling force by dynein and possibly other motors canceled each other out or were nonexistent), the total force pushed centrosomes away from the equator when they were close together and toward it when they were far apart (Figure 4B; Figure S3B). In this case, the model predicted a single stable separation between centrosomes where the force balances to zero. With realistic parameters and chromosome distribution in the midplane (see Supplemental Data and Table S2), this stable length was ~11 μm when Eg5 and dynein were both either active or inhibited (Figure 4B), a value that matched the spindle length observed in vivo under similar conditions (Table S1).

Less intuitively, the model revealed that when parameter *B* increased (i.e., when Eg5 alone was inhibited and there was a significant unopposed inward pulling force by dynein and possibly other motors), the total force on centrosomes exhibited more complex behavior (Figure 4B; Figure S3B). Although the force was still repulsive when centrosomes were close together and attractive when they were far apart, it did not simply decrease monotonically with distance. Rather, it became negative when centrosomes were separated by less than ~5 μm and positive when centrosomes were separated by ~5–11 μm. This is because below the ~5 μm threshold, antiparallel MT overlap ($\sim 2xe^{-2x/L}$) is large and the pulling action of dynein is dominant, whereas above the threshold, antiparallel MT overlap becomes smaller and the repulsive action generated by MTs interacting with chromosome arms overcomes the dynein-mediated attraction. As a result, the model predicted a stable separation of ~11 μm when the initial centrosomal separation was greater than ~5 μm and collapse when this separation was less than ~5 μm. The predicted bistability and length of Eg5-inhibited spindles, as well as the threshold distance, again matched well with the in vivo data (Table S1). Computer simulations of mobile centrosomes and chromosomes were also in agreement with the in vivo observations (Figures S6C and S6D; Movies S8 and S9).

Together, our in silico data accurately simulated our in vivo observations, regarding both the outcome of spindle assembly in the presence of Eg5 and dynein inhibitors and the length of the resulting spindles, and did so with dynein acting on overlapping MTs. Importantly, we varied the model's assumptions and parameters and established that if dynein were acting from the cell cortex, spindle poles, or chromosomes, rather than on antiparallel MTs, the virtual spindle behavior would be incompatible with our observations. Note that some of the modeling assumptions are not crucial: other repulsive interactions than those mediated by chromosome arms, other attractive forces than those brought about by kinetochore tension, and other MT length distributions than the exponential one still predict the same qualitative behavior that we observed. However, the action of dynein specifically on antiparallel MTs is essential.

Conclusions

Our in vivo and in silico results demonstrate that spindle collapse in the absence of functional Eg5 requires dynein activity and an initial intercentrosomal distance of less than ~5 μm, supporting our hypothesis that dynein opposes Eg5 by crosslinking and sliding antiparallel MTs. This represents a novel role for dynein during mammalian spindle assembly.

Because centrosome separation in prophase requires dynein, presumably anchored to the nuclear envelope acting on astral MTs, as well as Eg5 acting on antiparallel MTs [2, 23], we propose that as mitosis progresses and centrosomes separate, dynein becomes recruited to newly forming regions of antiparallel overlap where it can antagonize the activity of Eg5 and limit or stabilize centrosome separation so as to

prevent anaphase-like prometaphase [24]. With centrosomes stably separated, the capture of chromosomes by centrosomal MTs may be more efficient, thus enhancing chromosome biorientation and spindle assembly.

Experimental Procedures

Materials

All materials for cell culture were obtained from Sigma-Aldrich with the exception of Opti-MEM, which was obtained from Invitrogen, and fetal bovine serum, which was obtained from Atlanta Biologicals. Unless otherwise noted, all other chemicals were obtained from Sigma-Aldrich.

Cell Culture and Nocodazole Treatment

LLC-Pk1 cells expressing either GFP-tubulin or photoactivatable (PA) GFP-tubulin were cultured as previously described [7, 25]. Cells were plated on glass coverslips (Corning Inc. Life Sciences) or etched glass coverslips (BellCo Glass Co.) 2 days prior to imaging. For live imaging, cells were mounted in chambers containing non-CO_2 MEM supplemented with 0.3 U/ml Oxyrase (EC-Oxyrase, Oxyrase Inc.) and were maintained at ~37°C. Nocodazole treatment and 4× washouts were performed as previously described [12], except that 5–10 min incubations separated each washout.

Inhibitors

Monastrol was used at 200 μM. p150-CC1 plasmid was prepared according to protocol [26] and, following dilution with injection buffer (50 nM K-Glu, 1 mM $MgCl_2$, [pH 7.0]), was injected at 25 μM. Injection was performed on a Nikon Eclipse TE 300 inverted microscope using either a 60× or 100× phase objective lens and a PV820 Pneumatic PicoPump (World Precision Instruments). Needles were pulled from Omega Dot capillary glass tubes (Friedrich and Dimmock, Inc.) on a Brown-Flaming P-80 micropipette puller (Sutter Instrument Co.).

Immunofluorescence

LLC-Pk1 cells were rinsed twice in calcium- and magnesium-free phosphate-buffered saline ($PBS^{-/-}$), fixed in glutaraldehyde (0.25% glutaraldehyde in $PBS^{-/-}$), formaldehyde (3.7% formaldehyde in H_2O), paraglutaraldehyde (3.7% paraformaldehyde, 0.1% glutaraldehyde, and 0.5% Triton X-100 in $PBS^{-/-}$), or 100% methanol, and rehydrated in PBS containing 0.1% Tween and 0.02% sodium azide. The following primary antibodies were used in these experiments: γ-tubulin, used at 1:2000; Mad2, used at 1:200; and YL½ (Accurate Chemical), used at 1:2. Incubations with primary antibodies were performed overnight at room temperature or for 1 hr at 37°C. Cy3-labeled (Jackson ImmunoResearch Laboratories) or fluorescein isothiocyanate-labeled (Sigma-Aldrich) secondary antibodies were used at the recommended dilution for 30 or 90 min at room temperature, respectively. DNA was visualized with 4′,6-diamidino-2-phenylindole, used at 1:300. Coverslips were mounted in Vectashield (Vector Laboratories) and sealed with nail polish.

Image Acquisition

Images were acquired using a Nikon Eclipse TE 300 inverted microscope equipped with a 100× phase, NA 1.4 objective lens, a spinning-disk confocal scan head (PerkinElmer), and a Hamamatsu Orca ER cooled CCD camera (Hamamatsu). All images were taken with a dual-wavelength (488/568) filter cube. Image acquisition was controlled by Metamorph software (Molecular Devices). Time-lapse sequences were acquired at 5 s–2 min intervals with exposure times of 400–800 ms. Z stacks were acquired at 0.2 μm steps with similar exposure times. Photoactivation experiments were performed as previously described [27]. Images of fixed cells were acquired by capturing optical sections every 0.2 μm with exposure times of 400–600 ms (at 488 nm) and 600–800 ms (at 568 nm).

Modeling

The modeling was based on numerical solutions of the systems of differential equations described and explained in the Supplemental Experimental Procedures. The numerical analysis was done with standard MATLAB m-files; simulations were performed on a desktop computer.

Supplemental Data

Supplemental Data include Supplemental Experimental Procedures, six figures, two tables, and nine movies and can be found online at http://www.cell.com/current-biology/supplemental/S0960-9822(09)01705-9.

Acknowledgments

p150-CC1 plasmid was a kind gift of T. Kapoor (The Rockefeller University). Antibodies to Mad2 were a kind gift of A. Khodjakov (Wadsworth Center). We thank members of the Lee and Ross laboratories (University of Massachusetts Amherst) for insightful comments. This work was supported by grants from the National Institutes of Health (to A.M. and P.W.).

Received: April 24, 2009
Revised: September 2, 2009
Accepted: September 4, 2009
Published online: October 15, 2009

References

1. Blangy, A., Lane, H.A., d'Hérin, P., Harper, M., Kress, M., and Nigg, E.A. (1995). Phosphorylation by $p34^{cdc2}$ regulates spindle association of human Eg5, a kinesin-related motor essential for bipolar spindle formation in vivo. Cell *83*, 1159–1169.
2. Vaisberg, E.A., Koonce, M.P., and McIntosh, J.R. (1993). Cytoplasmic dynein plays a role in mammalian mitotic spindle formation. J. Cell Biol. *123*, 849–858.
3. Tanenbaum, M.E., Macůrek, L., Galjart, N., and Medema, R.H. (2008). Dynein, Lis1 and CLIP-170 counteract Eg5-dependent centrosome separation during bipolar spindle assembly. EMBO J. *27*, 3235–3245.
4. Sharp, D.J., McDonald, K.L., Brown, H.M., Matthies, H.J., Walczak, C., Vale, R.D., Mitchison, T.J., and Scholey, J.M. (1999). The bipolar kinesin, KLP61F, cross-links microtubules within interpolar microtubule bundles of *Drosophila* embryonic mitotic spindles. J. Cell Biol. *144*, 125–138.
5. Kapitein, L.C., Peterman, E.J., Kwok, B.H., Kim, J.H., Kapoor, T.M., and Schmidt, C.F. (2005). The bipolar mitotic kinesin Eg5 moves on both microtubules that it crosslinks. Nature *435*, 114–118.
6. van den Wildenberg, S.M., Tao, L., Kapitein, L.C., Schmidt, C.F., Scholey, J.M., and Peterman, E.J. (2008). The homotetrameric kinesin-5 KLP61F preferentially crosslinks microtubules into antiparallel orientations. Curr. Biol. *18*, 1860–1864.
7. Rusan, N.M., Fagerstrom, C.J., Yvon, A.M., and Wadsworth, P. (2001). Cell cycle-dependent changes in microtubule dynamics in living cells expressing green fluorescent protein-α tubulin. Mol. Biol. Cell *12*, 971–980.
8. Mayer, T.U., Kapoor, T.M., Haggarty, S.J., King, R.W., Schreiber, S.L., and Mitchison, T.J. (1999). Small molecule inhibitor of mitotic spindle bipolarity identified in a phenotype-based screen. Science *286*, 971–974.
9. Quintyne, N.J., Gill, S.R., Eckley, D.M., Crego, C.L., Compton, D.A., and Schroer, T.A. (1999). Dynactin is required for microtubule anchoring at centrosomes. J. Cell Biol. *147*, 321–334.
10. Inoué, S., and Salmon, E.D. (1995). Force generation by microtubule assembly/disassembly in mitosis and related movements. Mol. Biol. Cell *6*, 1619–1640.
11. Boleti, H., Karsenti, E., and Vernos, I. (1996). Xklp2, a novel Xenopus centrosomal kinesin-like protein required for centrosome separation during mitosis. Cell *84*, 49–59.
12. Tulu, U.S., Fagerstrom, C., Ferenz, N.P., and Wadsworth, P. (2006). Molecular requirements for kinetochore-associated microtubule formation in mammalian cells. Curr. Biol. *16*, 536–541.
13. Khodjakov, A., Cole, R.W., Oakley, B.R., and Rieder, C.L. (2000). Centrosome-independent mitotic spindle formation in vertebrates. Curr. Biol. *10*, 59–67.
14. Lončarek, J., Kisurina-Evgenieva, O., Vinogradova, T., Hergert, P., La Terra, S., Kapoor, T.M., and Khodjakov, A. (2007). The centromere geometry essential for keeping mitosis error free is controlled by spindle forces. Nature *450*, 745–749.
15. Heald, R., Tournebize, R., Blank, T., Sandaltzopoulos, R., Becker, P., Hyman, A., and Karsenti, E. (1996). Self-organization of microtubules into bipolar spindles around artificial chromosomes in *Xenopus* egg extracts. Nature *382*, 420–425.
16. Chakravarty, A., Howard, L., and Compton, D.A. (2004). A mechanistic model for the organization of microtubule asters by motor and non-motor proteins in a mammalian mitotic extract. Mol. Biol. Cell *15*, 2116–2132.
17. Gatlin, J.C., Matov, A., Groen, A.C., Needleman, D.J., Maresca, T.J., Danuser, G., Mitchison, T.J., and Salmon, E.D. (2009). Spindle fusion

requires dynein-mediated sliding of oppositely oriented microtubules. Curr. Biol. *19*, 287–296.

18. Han, G., Liu, B., Zhang, J., Zuo, W., Morris, N.R., and Xiang, X. (2001). The *Aspergillus* cytoplasmic dynein heavy chain and NUDF localize to microtubule ends and affect microtubule dynamics. Curr. Biol. *11*, 719–724.
19. Lee, W.L., Oberle, J.R., and Cooper, J.A. (2003). The role of the lissencephaly protein Pac1 during nuclear migration in budding yeast. J. Cell Biol. *160*, 355–364.
20. Kim, H., Ling, S.C., Rogers, G.C., Kural, C., Selvin, P.R., Rogers, S.L., and Gelfand, V.I. (2007). Microtubule binding by dynactin is required for microtubule organization but not cargo transport. J. Cell Biol. *176*, 641–651.
21. Faruki, S., Cole, R.W., and Rieder, C.L. (2002). Separating centrosomes interact in the absence of associated chromosomes during mitosis in cultured vertebrate cells. Cell Motil. Cytoskeleton *52*, 107–121.
22. Dogterom, M., and Leibler, S. (1993). Physical aspects of the growth and regulation of microtubule structures. Phys. Rev. Lett. *70*, 1347–1350.
23. Saunders, W.S., and Hoyt, M.A. (1992). Kinesin-related proteins required for structural integrity of the mitotic spindle. Cell *70*, 451–458.
24. Bajer, A.S. (1982). Functional autonomy of monopolar spindle and evidence for oscillatory movement in mitosis. J. Cell Biol. *93*, 33–48.
25. Tulu, U.S., Rusan, N.M., and Wadsworth, P. (2003). Peripheral, non-centrosome-associated microtubules contribute to spindle formation in centrosome-containing cells. Curr. Biol. *13*, 1894–1899.
26. King, S.J., Brown, C.L., Maier, K.C., Quintyne, N.J., and Schroer, T.A. (2003). Analysis of the dynein-dynactin interaction in vitro and in vivo. Mol. Biol. Cell *14*, 5089–5097.
27. Ferenz, N.P., and Wadsworth, P. (2007). Prophase microtubule arrays undergo flux-like behavior in mammalian cells. Mol. Biol. Cell *18*, 3993–4002.

Current Biology, Volume *19*

Supplemental Data

Dynein Antagonizes Eg5 by Crosslinking and Sliding Antiparallel Microtubules

Nick P. Ferenz, Raja Paul, Carey Fagerstrom, Alex Mogilner, and Patricia Wadsworth

Supplemental Experimental Procedures

Mathematical Model

Force Balance with Steady Chromosomal Configuration

The parameters and variables of the model can be found in Table S2. We assume that MTs nucleated at centrosomes display an exponential length distribution in accordance with a simple phenomenological model of dynamic instability [1]: $N(l) \propto e^{-l/L}$, where L is the average MT length. Placing the centrosomes at $\pm x$, we can count the antiparallel MT numbers overlapping at distance s from the spindle equator (Figure S6A). To overlap, MTs from the right and left have to be longer than $l = x - s$ and $l = s - (-x) = s + x$, respectively. The probability of such overlapping MTs is proportional to $e^{-(x-s)/L} \times e^{-(x+s)/L}$ and the total overlap length is proportional to the integral over the spindle length: $\int_{-x}^{x} e^{-(x-s)/L} \times e^{-(x+s)/L} ds = e^{-2x/L} \int_{-x}^{x} ds = 2xe^{-2x/L}$. The corresponding motor force on overlapping MTs is $-2Bxe^{-2x/L}$, where B is the net force (its positive sign corresponds to the inward force) that takes into account both inward (dynein-generated, B_{dyn}) and outward (Eg5-generated, B_{eg5}) forces: $B = B_{dyn} - B_{eg5}$. Assuming that dynein motors are localized at or near the MT plus ends (not along the whole overlap length) re-scales the constant B but does not change the functional dependence of the integral on x.

Calculating the distance-dependence of the chromosome arm force is even simpler. The maximal force, A, when the centrosome is immediately opposite to the

chromosome should decrease with distance as the number of MTs longer than this distance: $Ae^{-x/L}$. Assuming for simplicity that there is a functional kinetochore fiber with motors at the kinetochore generating a force-independent tension, *C*, the total force on the centrosomes symmetrically placed at distance *x* around a single chromosome has the form:

$$F(x) = Ae^{-x/L} - 2Bxe^{-2x/L} - C \qquad \text{(Eq. 1)}$$

We plotted this force-distance dependence in Figure S3B and found that for some values of parameters, the non-monotonic force-distance behavior causing instability is possible.

Eq. 1 has to be generalized to account for the interactions of centrosomes with multiple chromosomes. The images shown in Figure S2A suggest that chromosomes distribute within a disc at the spindle midplane. Thus, we used a random number generator to spread $N = 38$ chromosomes uniformly and randomly inside a cylindrical disc of width equal to 2μm and radius equal to 3.5μm (Figure S6B; average inter-chromosomal distance for such packing is ~2μm). Assuming additive action of the chromosomes, the total force on the centrosomes symmetrically placed at distance *x* around the spindle equator is:

$$F_{cent}(x) = -2Bxe^{-2x/L} + \sum_{j=1}^{N}\left[\frac{x - x_j}{R_j}\left(A\exp\left(-R_j / L\right) - C\right)\right], R_j = \sqrt{\left(x - x_j\right)^2 + r_j^2} \qquad \text{(Eq. 2)}$$

This is the *x*-component of the force; on average, the component of the force normal to the spindle axis is negligible. We used Eq. 2 to plot the force-distance relationship in Figure 4B. Note that in such a chromosomal configuration, where most of the chromosomes are not *exactly* at the pole-pole axis, the repulsive forces from the chromosome arms do not effectively push the centrosomes in the *x*-direction when centrosomes approach the equator: these repulsive forces become almost perpendicular to the pole-pole axis. This is the reason for the force on the centrosome dropping almost to zero when *x* decreases.

Calibrating the Model Parameters

The orders of magnitude of the model parameters can be approximated based on the following considerations. Indirect estimates based, for example, on Grill et al. [2] and Mastronarde et al. [3], but in fact on the vast number of guesses in the literature, suggest that there are of the order of hundred(s) of MTs per centrosome. Assuming that a maximum of ~5 MTs reaches for each chromosomal arm (adding up to 150-200 MTs), and that the MT pushing force is ~5pN [4-6], we estimate that the maximal chromosome arm force A = 25pN. Based on measured and estimated MT dynamic instability parameters [7-9], the average MT length is of the order of a few microns.

When L = 2.5μm, the model predicts that about 15% of the MTs can reach the spindle equator and overlap, so we can assume that on the order of 10 pairs of interpolar MTs overlap at the spindle equator. EM data [10] agree with this estimate. Assuming that a few motors of each kind act on one micron of the overlap, and that each motor generates pN-range force [11], we estimate roughly 25pN/μm force per unit length at the interpolar MT overlap. Assuming that ~10 pairs of interpolar MTs overlap at the spindle equator, we estimate maximal parameter B as 250pN/μm. In fact, it is a sum of the Eg5-generated outward motor force, B_{eg5}, the dynein-generated inward motor force, B_{dyn}, and possible additional inward motor force (e.g., kinesin-14 motors), each of which is thus ~100pN/μm.

More precisely, the force-related model parameters can be calibrated using quantitative restrictions from the observations. First, when centrosomes are collapsed, chromosomes arrange themselves roughly on a surface of a sphere of radius R ~7μm around the collapsed centrosomes. When N = 38, chromosomes are uniformly radially distributed, the average distance between two adjacent chromosomes is ~ $\sqrt{4\pi R^2/3N} \sim 2R/\sqrt{N} \sim 2\,\mu\text{m}$, and the inter-chromosome interactions can be neglected (see below). The condition of the balance between the repulsive chromosomal arm force and the attractive kinetochore force per chromosome is $A\exp(-R/L) - C = 0$, thus:

$$C = A\exp(-R/L) \qquad \text{(Eq. 3)}$$

Using parameter A = 5 (one unit of force was 25pN, so A = 5 corresponds to A = 125pN), R = 7μm and $C = A\exp(-R/L)$, we used the following formula derived from Eq. 2 to plot the force-density relation (Figure 4B) in the case of both uninhibited and co-inhibited (Eg5- and dynein-inhibited) cells, when parameter B = 0:

$$F_{cent}(x) = \sum_{j=1}^{N}\left[\frac{x-x_j}{R_j}\left(A\exp(-R_j/L) - A\exp(-R/L)\right)\right], R_j = \sqrt{(x-x_j)^2 + r_j^2} \qquad \text{(Eq. 4)}$$

The results, remarkably robust with respect to varying the average MT length L, give the average stable spindle length ~10.8 ± 0.3μm, agreeing very well with the experimental data (Table S1).

A simple reason that the predicted spindle length is less than the 14μm ($2R$) that would be expected if all chromosomes are exactly at the middle of the pole-pole axis is that the chromosomes are spread in the midplane, so the effective repulsion from the more distal chromosomes is smaller. Note that some randomness is introduced due to the random localization of the individual chromosomes at the midplane. However, because many chromosomes are packed together, this randomness is small, and the stability of the single spindle steady state never changes. The stable spindle length goes up (or down) if the chromosomes are spread more widely along (or perpendicular to) the spindle axis, but this effect is relatively small. However, this effect can nicely explain the slight (11 to 12μm) elongation of the co-inhibited spindle compared to the uninhibited one: note respective widening of the chromosomal 'cloud' along the spindle axis in Figure S2A.

In the Eg5-inhibited cell, $B = B_{dyn} > 0$, and the spindle has the following bistability property: if the initial intercentrosomal distance is below ~5.5μm, the centrosomes collapse together, while if the initial intercentrosomal distance is above ~5.5μm, the centrosomes separate to the stable spindle length of ~11μm (Table S1). We used the equation:

$$F_{cent}(x) = -2B_{dyn}xe^{-2x/L} + \sum_{j=1}^{N}\left[\frac{x-x_j}{R_j}\left(A\exp\left(-R_j/L\right) - A\exp\left(-R/L\right)\right)\right], R_j = \sqrt{\left(x-x_j\right)^2 + r_j^2} \quad \text{(Eq. 5)}$$

to plot the force-density relation (Figure 4B) and found that for reasonable values of L, we could find a range of values of B_{dyn} for which the bistability property is captured (e.g., for $L = 2, B_{dyn} = 2.5; L = 3, B_{dyn} = 1.5; L = 4, B_{dyn} = 1$). We found that for these parameter values (we also widened the chromosomal 'cloud' along the spindle axis from 2μm to 4μm), Eq. 5 predicts the correct stable spindle length and the threshold length beneath which the spindle collapses (~5μm), only slightly lower than that observed (~5.5μm). Finally, the model predicts that for the dynein-inhibited cell (Eq. 5 has to be used with $B_{eq} = -B_{dyn}$ instead of B_{dyn}), the stable spindle length is again ~11μm.

Mobile Chromosomes

When we tested the net forces on the centrosomes in the directions perpendicular to the pole-pole axis, it became clear that the centrosomes could actually be destabilized by lateral displacements. This indicates that centrosomes and chromosomes both must be mobile during computer simulations in order to predict possible stable spindle configurations (Figures S6C and S6D; Movies S8 and S9); however, this makes mathematical analysis forbidding, and we resorted to solving equations of movements numerically. Eq. 2 can be re-written as follows:

$$F_{cent}(\vec{x}) = B(\vec{y}-\vec{x})\exp\left(-\left|\vec{y}-\vec{x}\right|/L\right) + \sum_{j=1}^{N}\left[\frac{\vec{y}-\vec{z}_j}{\left|\vec{y}-\vec{z}_j\right|}\left(A\exp\left(-\left|\vec{y}-\vec{z}_j\right|/L\right) - C\right)\right] \quad \text{(Eq. 6)}$$

where $\vec{x}$ and $\vec{y}$ are the coordinates of two centrosomes in space, and $\vec{z}_j$ is the position of the j-th chromosome. To simulate chromosomal movements, we introduced inter-chromosomal interactions assuming that the force between a pair of chromosomes has the form:

$$F_{chr}\left(\vec{z}_i\right)=\sum_{j=1}^{N}\left[\frac{\vec{z}_i-\vec{z}_j}{\left|\vec{z}_i-\vec{z}_j\right|}\Phi\left(\left|\vec{z}_i-\vec{z}_j\right|\right)\right]$$
$$-\frac{\vec{y}-\vec{z}_i}{\left|\vec{y}-\vec{z}_i\right|}\left(A\exp\left(-\left|\vec{y}-\vec{z}_i\right|/L\right)-C\right)-\frac{\vec{x}-\vec{z}_i}{\left|\vec{x}-\vec{z}_i\right|}\left(A\exp\left(-\left|\vec{x}-\vec{z}_i\right|/L\right)-C\right) \quad \text{(Eq. 7)}$$

Here, the two last terms describe the force between the *i*-th chromosome and the centrosomes, while the sum is responsible for the pair-wise inter-chromosomal repulsion (both steric and mediated by the MTs and motors):

$$\Phi\left(z_{ij}\right)=\begin{cases}D\left(z_{rep}-z_{ij}\right) & z_{ij}<z_{rep}\\ 0, & z_{ij}>z_{rep}\end{cases}, \quad \text{(Eq. 8)}$$

so that the chromosomes do not interact beyond a certain distance z_{rep}, and the repulsion linearly grows to a certain force *D* as the inter-chromosomal distance decreases.

We describe the movements of the centrosomes and chromosomes with usual mechanics equations in the over-damped regime within the cell [4, 5]:

$$\frac{d\vec{x}}{dt}=\frac{1}{\zeta_{cent}}F_{cent}\left(\vec{x}\right),\frac{d\vec{y}}{dt}=\frac{1}{\zeta_{cent}}F_{cent}\left(\vec{y}\right),\frac{d\vec{z}_i}{dt}=\frac{1}{\zeta_{chr}}F_{chr}\left(\vec{z}_i\right) \quad \text{(Eq. 9)}$$

so that the velocities of the centrosomes and chromosomes are proportional to respective forces divided by the effective drag coefficients.

We assume that chromosomes repel each other when they are closer than z_{rep} = 2μm (about their size) from each other, and that their maximal repulsion *D* is 50pN (tens of pN is the characteristic magnitude of the spindle forces [4, 5]. Changing these two parameters by an order of magnitude either way does not alter the predicted behavior. Near equilibrium, the force restoring the stable pole-pole separation has the linear spring-like behavior (Figure 4B): $F\approx 50pN\times\left(-s/2\mu m\right)$, where *s* is the displacement from the equilibrium. Solving the equation of motion near the equilibrium: $ds/dt=F/\zeta_{cent}$, we

obtain $s \propto \exp(-t/\tau)$ and calculate the relaxation time $\tau = \zeta_{cent} \times 2\mu m / 50 pN$. Our observations of the rate of the spindle length change near the equilibrium suggest that the characteristic relaxation time is $\tau \sim 100 \sec$, which gives the estimate for the centrosome drag coefficient: $\zeta_{cent} \sim 2500 pN \times \sec/\mu m$. Assuming that because of the smaller size of the chromosome, its drag coefficient is 10 times smaller than that of the centrosomal MT aster [4, 5], we estimate $\zeta_{chr} \sim 250 pN \times \sec/\mu m$. These estimates are higher, but of the same order of magnitude as those made for the *Drosophila* spindles [4, 5]. Interestingly, we found that chromosomes actually do have to be much more mobile (less resistant to force) than the centrosomes in order for the simulations to predict non-collapse of well-separated centrosomes in Eg5-inhibited cells. Otherwise, the centrosomes collapse before chromosomes converge to the spindle equator and generate enough repulsion.

We solved Eqs. 6-9 numerically in 2D with parameters L = 4-6μm, $A = 1, C = 0.06, \quad B_{eg5} = B_{dyn} = 0.7 - 1$ and obtained the behavior semi-quantitatively mimicking the observations (Figures S6C and S6D; Movies S8 and S9) and agreeing with the predictions of the simplified force-distance calculations with the immobile chromosomes.

Model Limitations and Simplifications

Our model makes a number of significant simplifications: (i) we assume that all kinetochore fibers and interpolar MT bundles are assembled at once, while in reality this process takes time, during which the centrosomes and chromosomes start to move; (ii) we neglect the geometric effects of chromosomes 'screening' each other out (in fact, clearly, not all chromosomes interact with the centrosomes equally); (iii) we assume that MT dynamics are fast, and so are in quasi-equilibrium with current centromes' and chromosomes' positions; (iv) we neglect stochastic fluctuations of forces due to significant randomness of the relatively small MT number; (v) it is not clear whether kinetochore fiber tension is length-independent; (vi) there are likely deviations from the exponential MT length distribution, and we ignore the geometric effect of the MT density decrease in 3D; (vii) we simulate the movements in 2D, because in 3D the numerical

simulations become too time-consuming; and (viii) we include only active, force generating motor proteins at the MT overlap, not passive crosslinking proteins.

These limitations do not change the model's conclusions qualitatively. A number of simulations (not systematic ones) showed that changing assumptions i, ii, v, vii and viii do not change qualitative model predictions. Likewise, spreading the MT bundle assembly in time, prohibiting some chromosomes in the middle from interacting with centrosomes, assuming that the kinetochore fiber tension is spring-like, trying different MT length distributions (i.e., piece-wise linear), adding viscous-like 'protein friction' generated by passive crosslinkers at the MT overlap and allowing centrosomes to move in 3D (keeping fixed 'spherical cloud-like' 3D chromosomal arrays) did not make a qualitative difference for the stability conditions of the centrosomal separation. Assumption (iii) is supported by the argument that the characteristic time for the MT dynamic cycle, ~25sec, estimated as the characteristic MT length (~5μm) divided by the growth/shrinkage rate (~0.2μm/sec) [7], is much shorter than the characteristic time of the spindle dynamics that is in a few minutes range. We discuss how the results could change if assumption (vi) is altered below. Finally, our previous experience with introducing stochastic dynamics [4, 5, 8] suggests that though it can significantly change the transient behavior, it is unlikely to alter the stability of the steady states qualitatively.

Mathematical Argument for Dynein Acting at Interpolar MT Overlap

The model has to account for the observation that when Eg5 is inhibited, the spindle is bistable. Assuming in this case that the dominant forces acting on the centrosomes are kinetochore MT tension (*Force C*), effective repulsion through MTs interacting with chromosomal arms (*Force A*), and force generated by dynein motors on chromosome-associated structures interacting with centrosomal MTs, the force on the centrosomes as a function of the spindle pole-equator distance x has the form: $F(x) = Af(x) - B_{dyn} f(x) - C$, where $f(x)$ is the distance dependence of the force, which in our case is proportional to the number of centrosomal MTs reaching the chromosomal arms. But if dynein is on the chromosome-associated structures, then a proportional number of MTs would reach for these dynein motors (and generate attraction) and for either chromokinesins, or simply chromosome arms (and generate repulsion), so the

$f(x)$ factor is the same for the repulsive and dynein forces. Thus, $F(x)=(A-B_{dyn})f(x)-C$, and the only way such force-distance dependence can account for the bistability is if function $f(x)$ has a maximum at a finite distance *x*. This is highly unlikely, as the number of MTs that can reach from the centrosome to the chromosomes surely increases when the centrosome-chromosome distance decreases. One can imagine that the repulsive force is not MT-number limited, but rather motor(chromokinesin)-number limited, in which case the bistability can be achieved without Eg5 and with dynein on the chromosomes. This is unlikely though because of the polymerization force, which has to be MT-number limited. Thus, it is unlikely that the data can be explained based on the force-balance model without dynein acting from the interpolar MT overlaps.

Effects of Various MT Length and Overlap Distributions

We assume that the overlapping interpolar MTs are scarce, even for the majority population of MTs from the proximal pole, and so the probability of the encounter of two MTs of opposite polarity is proportional to the product of the densities, rather than to the minority density from the distal pole. One argument for this assumption is that if the average MT length is significantly smaller than the spindle length, then near the equator the MT numbers are small enough. Besides, EM data from [10] shows that the overlapping MT bundles are not noticed far from the equator, and at the equator they consist of rarified bundles consisting of 2-4 MTs. All this said, it is indeed possible that if the MT populations are great, then the overlapping density is proportional to that of just minority population.

In that case, we cannot have bistability providing exponential decrease of the chromosomal MT lengths. Indeed, it is easy to compute that if the overlap is proportional to $G(x,s)=\min\left\{e^{-(x-s)/L},e^{-(x+s)/L}\right\}$, then the total overlap length is proportional to the integral over the spindle length: $\int_{-x}^{x}G(x,s)ds\sim Le^{-x/L}\left(1-e^{-x/L}\right)$. This function decreases exponentially with approximately the same speed as the effective centrosomal-chromosomal repulsion $\sim e^{-x/L}$, and under these conditions the bistability is impossible.

However, if the chromosomal MTs are much longer than the interpolar MTs, then the effective centrosomal-chromosomal repulsion $\sim 1/x^2$. In that case, the force-distance dependence has the form: $F(x) = A/x^2 - Be^{-x/L} - C$, and the bistability is possible. The general necessary condition for the spindle bistability is that the distance dependence of the effective repulsive centrosomal-chromosomal forces is different from that of the overlap length, so that the overlap distance-dependence function decreases faster than the effective repulsion at large distances, but can be greater than the repulsion at moderate distances.

It is also possible that the MT length distribution is not exponential. In fact, short MT depletion in the spindle was observed [11]. This property does not change the model conclusion: the reason is that the key feature guaranteeing the bistability is that the overlapping interpolar MT density decreases faster than the density of the astral/chromosomal MTs, which is the property of the *longer* MTs in the populations. Indeed, the MT length distribution observed in [11] can be approximated by the function $\sim\left(e^{-x/L} - e^{-x/l}\right)$, where $L > l$. In this case, the overlap is proportional to $G(x,s) = \left(e^{-(x-s)/L} - e^{-(x-s)/l}\right) \times \left(e^{-(x+s)/L} - e^{-(x+s)/l}\right)$, then the total overlap length is proportional to the integral over the spindle length: $H(x) = \int_{-x}^{x} G(x,s)ds \sim \left(2x - \frac{Ll}{L-l}\right)e^{-2x/L} + \left(2x + \frac{Ll}{L-l}\right)e^{-2x/l}$, and it is easy to check that the function $F(x) = Ae^{-x/L} - BH(x) - C$ has one stable zero for negative and small positive values of *B*, and also predicts the bistable spindle property for moderate positive values of *B*.

Other Possible Force-Generating Motors

Kinesin-14 (Ncd) motors, as noted in the text, can also contribute to the force generation at the antiparallel MT overlaps [4, 5]. This does not change the model predictions: adding such motors would add one additional parameter (B_{ncd}) to the net force density parameter $B = B_{dyn} + B_{ncd} - B_{eg5}$. Fitting the data with one additional parameter becomes

easier, of course. We observed that we can reasonably fit all observations with $B \approx 0$ and having values of B_{dyn}, B_{ncd} of the same order of magnitude.

Effects of Shorter and/or Parallel Overlapping MTs

On parallel MTs, multiple dynein motors would probably bind in such a way that about half of the motors have their binding domain on one MT and motor domain pulling on another, and another half in the opposite order. Both sub-populations would pull toward their respective minus ends thus generating forces in the opposite directions. As a result, these two motors' sub-populations cancel each other's forces, effectively just crosslinking the MTs and not generating any significant sliding force. The Eg5 motors, with motor domains on both ends, would simply 'walk' to the parallel plus ends. These motors would not generate any force if there is no relative sliding of the crosslinked pair of MTs. If there is such sliding, the motors on the parallel MTs would exert an 'anti-shearing' force trying to stop the sliding (and so will dynein motors).

If many parallel and antiparallel MTs are densely crosslinked by various motors, then these anti-shearing forces effectively 'lock' the parallel MTs together [12]. In this case our model holds, as far as the distribution of MT length density decreases monotonically from the poles to the equator of the spindle, and other assumptions about the overlap lengths and effective repulsive forces are valid. Finally, if the spindle is organized in a 'barrel'-like fashion [13] (Figure S6E), then force balance calculations reported in [14] predict that the parallel MT overlaps closer to the poles result in minus ends of the antiparallel MTs at the equator sliding outward toward respective poles. This MT flux partially (up to a few tens of percent) dampens the forces generated by the motors at the antiparallel MT overlaps at the equator, but does not change the distance dependence of the forces in Eq. 1, and so all model conclusions remain valid.

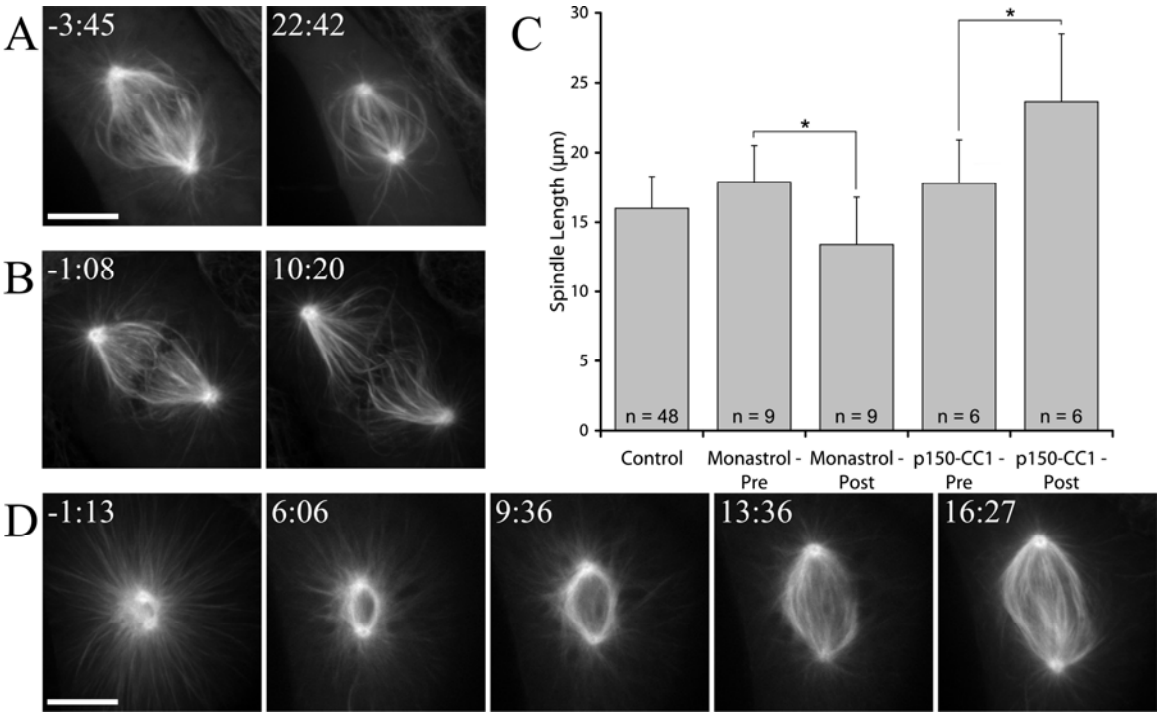

Figure S1. Eg5/Dynein Antagonism

Eg5 (A) and dynein (B) inhibition inversely affect metaphase spindle length. Images are maximum intensity projections, prior to (left) and following (right) motor inhibition.

(C) Average spindle length before and after each treatment + standard deviation. Data are significant (asterisks) at $p = 0.01$ (monastrol) and $p = 0.05$ (p150-CC1).

(D) Selected images from a time-lapse series of a monastrol-treated cell containing a monopolar spindle that was subsequently injected with p150-CC1 (Movie S1). This spindle bipolarizes within 20min. The first and last images are maximum intensity projections. All times are relative to motor inhibition (0:00) and are displayed as min:sec. Bars = 10µm.

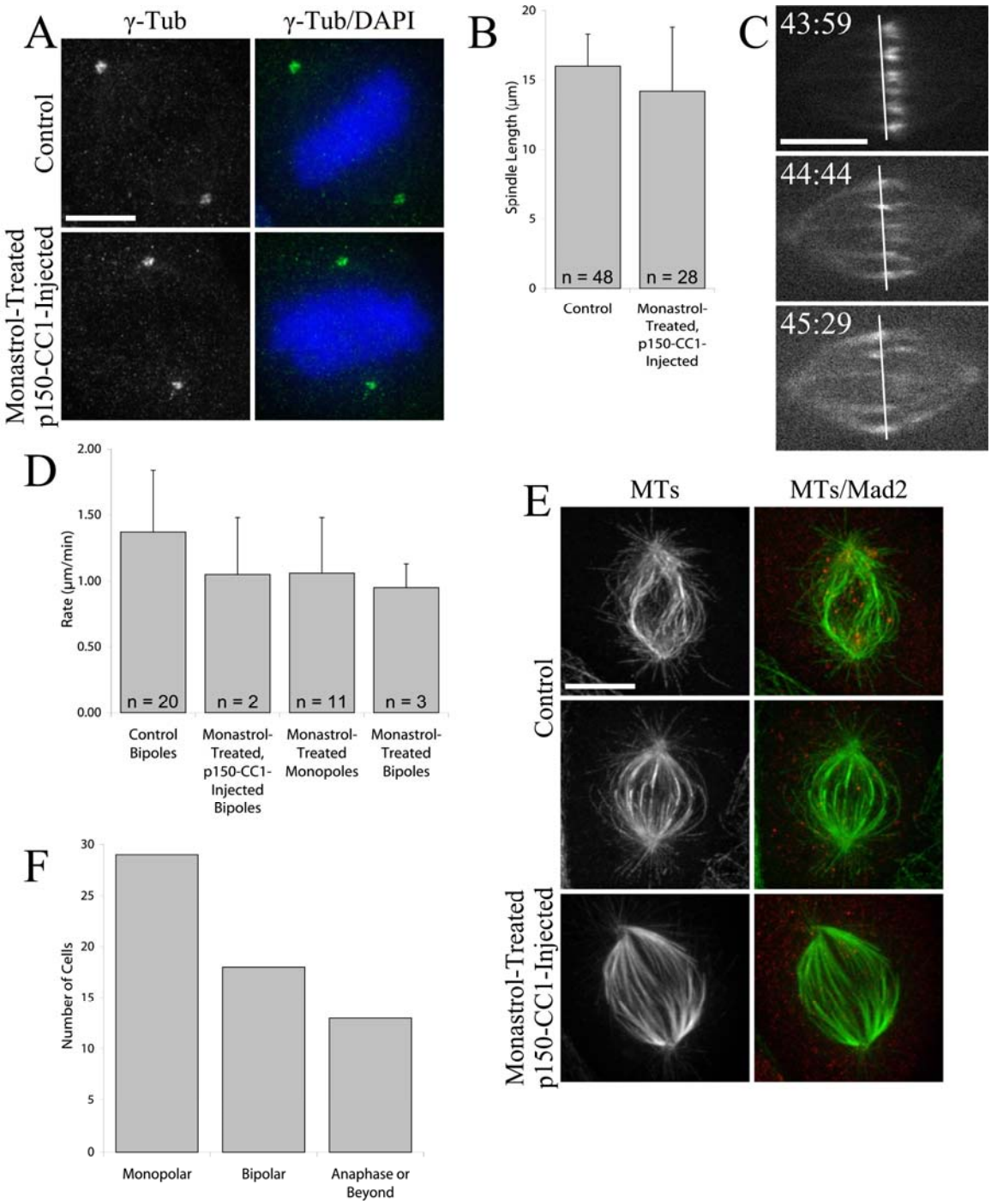

Figure S2. Morphology and Functionality of Eg5- and Dynein-Inhibited Bipolar Spindles

(A) Co-inhibited cells establish bipolarity via centrosome separation. Control (top) and monastrol-treated, p150-CC1-injected (bottom) LLC-Pk1 cells were fixed at metaphase and stained for γ-tubulin (left). A merge with DAPI is shown on the right.

(B) Average spindle length + standard deviation after the indicated treatments. Data are not statistically different.

(C and D) Co-inhibited spindles undergo MT flux at rates consistent with the inactivation of Eg5.

(C) Selected images from a time-lapse series of a monastrol-treated and p150-CC1-injected LLC-Pk1-PAα cell photoactivated parallel to the metaphase plate. The white lines serve as a fiduciary mark. Times are relative to injection (0:00) and are displayed as min:sec.

(D) Average rate of poleward flux + standard deviation after the indicated treatments. Values for control bipoles, monastrol-treated monopoles and monastrol-treated bipoles are from Ferenz and Wadsworth (2007).

(E) Co-inhibited spindles remove Mad2 from metaphase kinetochores. Control prometaphase (top), metaphase (middle) and monastrol-treated, p150-CC1-injected metaphase (bottom) LLC-Pk1 cells were fixed and stained for MTs (left). A merge with Mad2 is shown on the right.

(F) Mitotic fate of monastrol-treated and p150-CC1-injected monopoles. LLC-Pk1 cells were treated with monastrol, injected with p150-CC1, and then fixed and stained 1-5hrs post-injection. Cells that had previously been injected were located, and the mitotic stage of these cells was scored. Bars = 10μm.

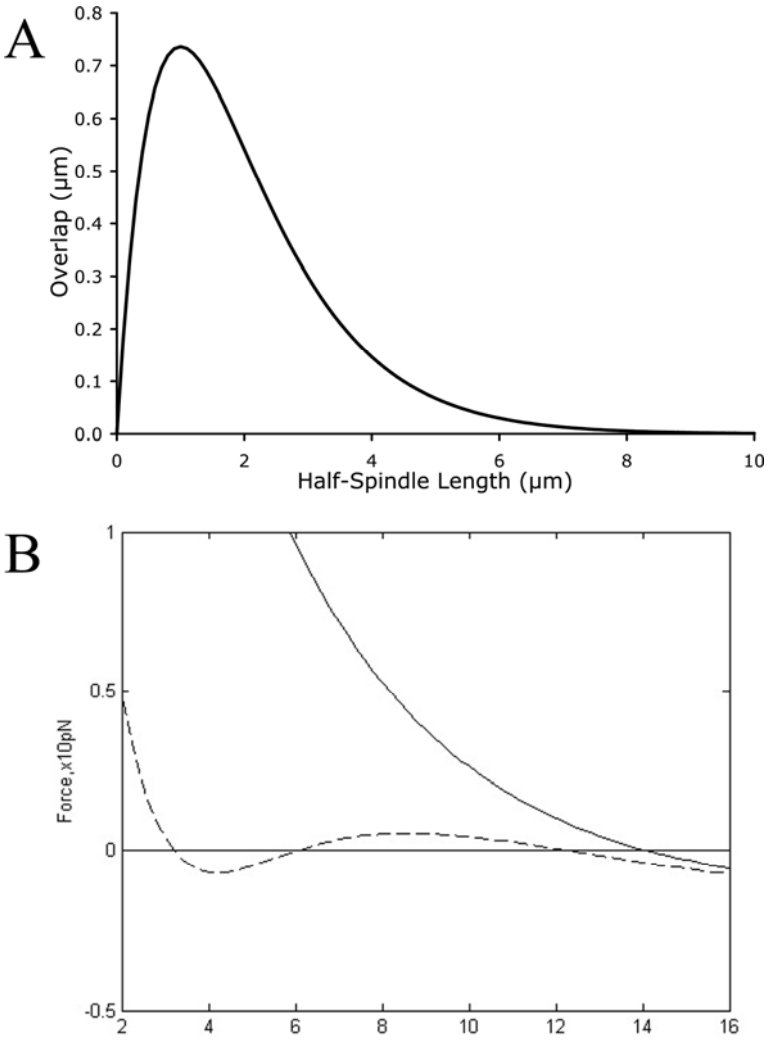

Figure S3. Antiparallel Overlap and Spindle Length Predictions

(A) A plot of antiparallel overlap with respect to the half-spindle length, according to $y = 2xe^{-2x/L}$ (see Supplemental Text). Here, $L = 2.0\mu m$.

(B) Force versus intercentrosomal distance given by the simplified model for $L = 2$; $A = 1$; $C = 0.03$ for uninhibited, co-inhibited (Eq. 1 in Supplemental Text, solid curve, $B = 0$) and Eg5-inhibited (Eq. 1 in Supplemental Text, dashed curve, $B = 0.65$) cells.

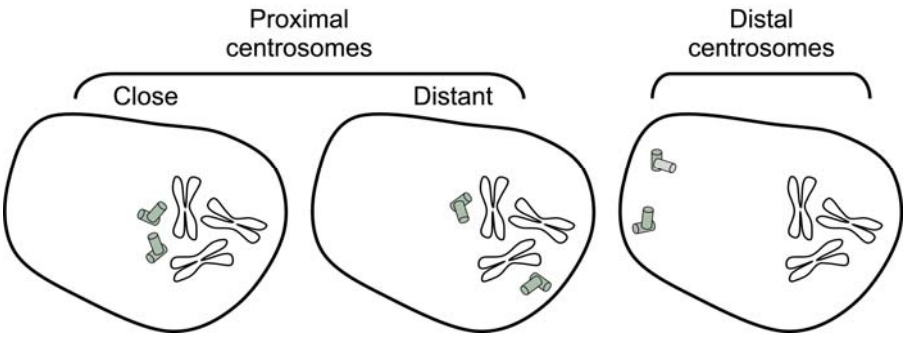

Figure S4. Centrosomal Distributions Created by Nocodazole Treatment

Schematic diagram illustrating three broad centrosomal configurations typically produced after treatment with nocodazole. Centrosomes are proximal when their MT arrays are able to interact with the chromosomal array after release from nocodazole; centrosomes are distal when they cannot. From cell to cell, the position of proximal centrosomes relative to one another is highly variable at the onset of spindle assembly. To categorize this variability, proximal centrosomes were classified as either close (< 5.5μm apart) or distant (> 5.5μm apart) (see Results and Discussion).

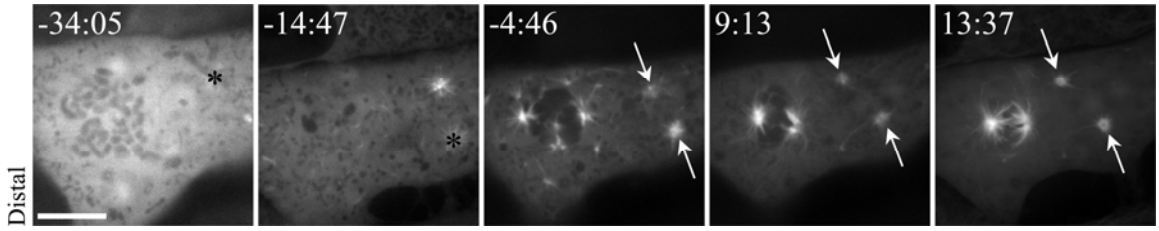

Figure S5. Acentrosomal Spindle Assembly Does Not Require Dynein Activity

Selected images from a time-lapse sequence of a cell treated with nocodazole, injected with p150-CC1 and then released from the drug. Here, a bipolar spindle assembles following nocodazole washout. Set up is as defined in Figure 2. Bar = 10μm.

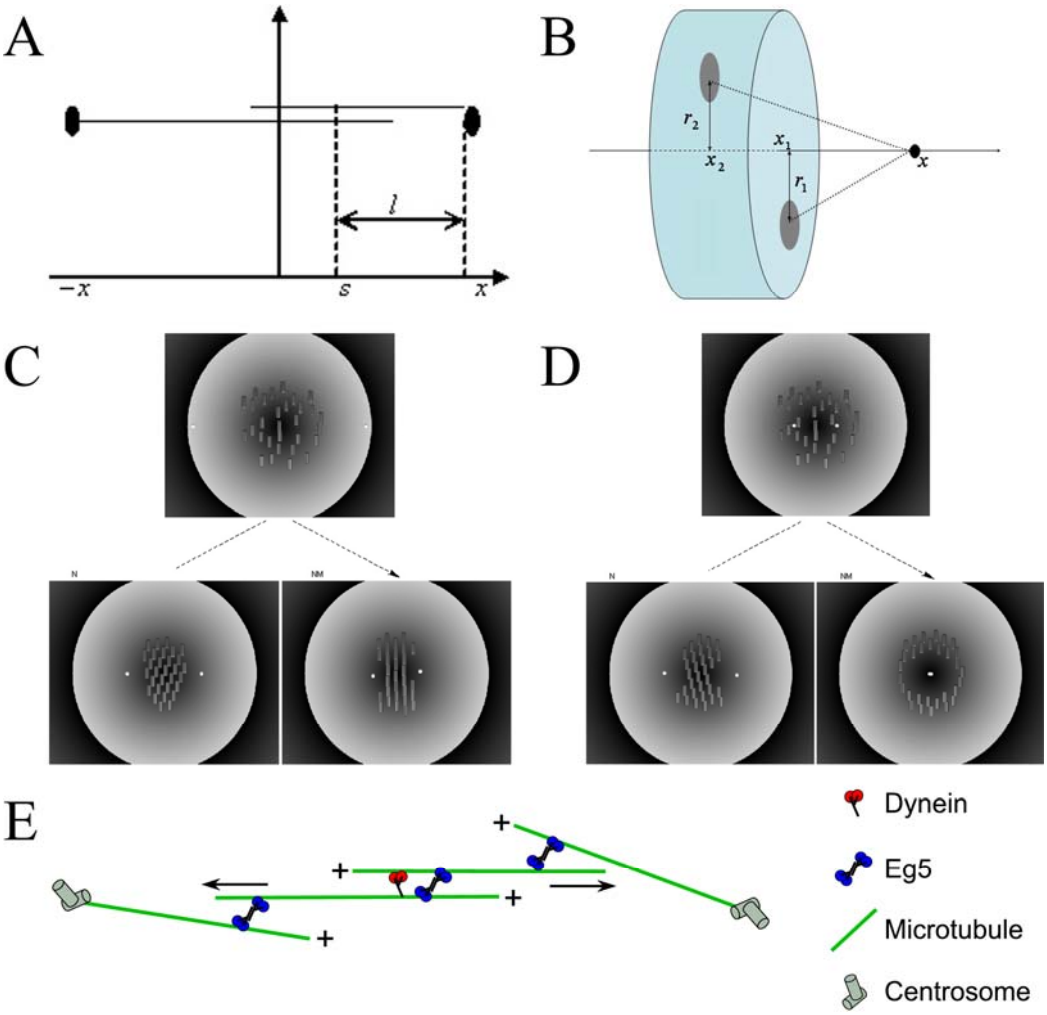

Figure S6. Interpolar Overlap, Force Calculations and Simulations

(A) Schematic illustrating how interpolar MT overlap was calculated.

(B) $N = 38$ chromosomes are distributed randomly and uniformly over the disc of width 2μm and radius 3.5μm in the spindle midplane.

(C and D) Simulations allowing centrosome and chromosome mobility in response to forces between them.

(C) Snapshots from simulated movements with proximal centrosomes far from one another. Top (initial configuration), bottom left (final configuration in uninhibited cells released from nocodazole, N), bottom right (final configuration in Eg5-inhibited cells released from nocodazole, NM; Movie S8). Note the difference in the chromosomal distribution in the bottom right image; here, inward pulling by interpolar MTs push the chromosomes outward from the equator.

(D) Same as C, except with proximal centrosomes close to one another. In uninhibited cells (bottom left), the centrosomes separate, albeit to a slightly less degree than from the greater initial separation, while in the Eg5-inhibited case (bottom right), the centrosomes collapse and are surrounded by a symmetric radial chromosomal distribution (Movie S9). (E) Schematic illustration of the 'barrel'-like spindle. Arrows show MT flux.

Table S1. Average Spindle Lengths

	Centrosomal spindle length (μm)	Acentrosomal spindle length (μm)
Control	10 ± 2	7 ± 1
Monastrol	11 ± 2	6 ± 2
Monastrol and p150-CC1	12 ± 2	6 ± N/A

Table S2. Model Parameters and Variables

Model Parameters

Notation	Meaning	Value
N	Number of chromosomes	38[a]
L	Average MT length	2 - 6μm[b]
A	Maximal chromosome arm force	25pN[c]
C	Kinetochore tension force	1 - 20pN[c]
B_{eg5}	Eg5-generated outward force at MT overlap	~100pN/μm[c]
B_{dyn}	Dynein-generated inward force at MT overlap	~100pN/μm[c]
D	Inter-chromosomal repulsion	~50pN[b]
z_{rep}	Distance at which chromosomes repel each other	~2μm[b]
ζ_{cent}	Effective centrosome drag coefficient	~2500pN×sec/μm[c]
ζ_{chr}	Effective chromosome drag coefficient	~250pN×sec/μm[c]

Model Variables

$\vec{x}, \vec{y}$	Coordinates of the centrosomes
$\vec{z}_i, i = 1...N$	Coordinates of the chromosomes

Quantitative Observations Used to Calibrate the Model Parameters

R	Distance between chromosomes and collapsed centrosomes	~7μm
L_u	Spindle length in an uninhibited cell	~11μm
L_{eg5}	Spindle length in an Eg5-inhibited cell	~11μm
L_{thr}	Threshold length beneath which the spindle collapses in an Eg5-inhibited cell	~5.5μm
L_{co}	Spindle length in a co-inhibited cell	~11μm
τ	Time of characteristic centrosome movement (by a few microns)	~100sec

Values were [a]determined from experiment, [b]assumed or [c]estimated.

Supplemental References

1. Dogterom, M., and Leibler, S. (1993). Physical aspects of the growth and regulation of microtubule structures. Phys. Rev. Lett. *70*, 1347-1350.
2. Grill, S.W., Howard, J., Schäffer, E., Stelzer, E.H., and Hyman, A.A. (2003). The distribution of active force generators controls mitotic spindle position. Science. *301*, 518-521.
3. Mastronarde, D.N., McDonald, K.L., Ding, R., and McIntosh, J.R.. 1993. Interpolar spindle microtubules in PtK cells. J. Cell Biol. *123*, 1475-1489.
4. Cytrynbaum, E.N., Scholey, J.M., and Mogilner, A. (2003). A force balance model of early spindle pole separation in *Drosophila* embryos. Biophys. J. *84*, 757-769.
5. Wollman, R., Civelekoglu-Scholey, G., Scholey, J.M., and Mogilner, A. (2008). Reverse engineering of force integration during mitosis in the *Drosophila* embryo. Mol. Syst. Biol. *4*, 195.
6. Dogterom, M., and Yurke, B. (1997). Measurement of the force-velicity relation for growing microtubules. Science. *278*, 856-860.
7. Rusan, N.M., Tulu, U.S., Fagerstrom, C., and Wadsworth, P. (2002). Reorganization of the microtubule array in prophase/prometaphase requires cytoplasmic dynein-dependent microtubule transport. J. Cell Biol. *158*, 997-1003.
8. Wollman, R., Cytrynbaum, E.N., Jones, J.T., Meyer, T., Scholey, J.M., and Mogilner, A. (2005). Effeicient chromosome capture requires a bias in the 'search-and-capture' process during mitotic spindle assembly. Curr. Biol. *15*, 828-832.
9. Cheerambathur, D.K., Civelekoglu-Scholey, G., Brust-Mascher, I., Sommi, P., Mogilner, A., and Scholey, J.M. (2007). Quantitative analysis of an anaphase B switch: predicted role for a microtubule catastrophe gradient. J. Cell Biol. *177*, 995-1004.
10. Sharp, D.J., McDonald, K.L., Brown, H.M., Matthies, H.J., Walczak, C., Vale, R.D., Mitchison, T.J., and Scholey, J.M. (1999). The bipolar kinesin, KLP61F, cross-links microtubules within interpolar microtubule bundles of *Drosophila* embryonic mitotic spindles. J. Cell Biol. *144*, 125-138.

11. Yang, G., Houghtaling, B.R., Gaetz, J., Liu, J.Z., Danuser, G., and Kapoor, T.M. (2007). Architectural dynamics of the meiotic spindle revealed by single-fluorophore imaging. Nat. Cell Biol. *9*:1233-1242.
12. Zemel, A., Mogilner, A. (2009). Motor-induced sliding of microtubule and actin bundles. Phys. Chem. Chem. Phys. *11*:4821-4833.
13. Yang, G., Cameron, L.A., Maddox, P.S., Salmon, E.D., and Danuser, G. (2008). Regional variation of microtubule flux reveals microtubule organization in the metaphase meiotic spindle. J. Cell Biol. *182*:631-639.
14. Brust-Mascher, I., Civelekoglu-Scholey, G., Kwon, M., Mogilner, A., and Scholey, J.M. (2004). Model for anaphase B: Role of three mitotic motors in a switch from poleward flux to spindle elongation. Proc. Natl. Acad. Sci. *101*:15938-15943.